Multi-Event Analysis of Super Equatorial Plasma Bubbles

Alanah Cardenas-O'Toole and Shasha Zou

University of Michigan Department of Climate and Space Sciences and Engineering

EQIT-14

Email: alanahco@umich.edu

Introduction

Equatorial Plasma Bubbles (EPBs) are one of the most severe ionospheric phenomena regarding the creation of amplitude and phase scintillations of radio signals. Generally, EPBs remain close to the magnetic equator, not usually varying more than 15 to 20 degrees from it. **When EPBs extend into midlatitudes (greater than +/- 25 ° Mlat), they are called Super Equatorial Plasma Bubbles (Super EPBs).** However, it is not known how often this phenomenon occurs or under what solar and geomagnetic activity conditions cause such an expansion and the scintillations they induce. In this analysis, multiple super EPB events are explored and analyzed using the Swarm satellite constellation, VISTA TEC, GOLD, and OMNI solar wind data to better understand the nature of Super EPBs.

Background

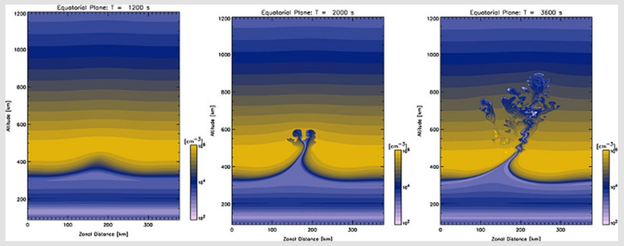

Figure 1. Simulation of the growth of an Equatorial Plasma Bubble (Yokoyama et al., 2014)

EPBs are regions usually in the low latitudes/ equator where there is a depleted segment of plasma density in the ionosphere. They occur most often during the postsunset (18-24 LT) and postmidnight (0-6 LT) hours, when the E-Region ionosphere is not present (Aa et al., 2020b). Gravity waves, enhanced zonal eastward electric fields, neutral wind shear, and nighttime medium-scale traveling ionospheric disturbances (MSTIDs) have been suggested as seeding mechanisms for triggering plasma bubbles, which are thought to be **a result of the generalized Rayleigh-Taylor (R- T) instability** (Sultan 1996).

The EPB is shown growing over time in Figure 1 (Yokoyama et al., 2014). The blue shows the low density, and the yellow shows the high density. A small perturbation can grow significantly because of an unstable equilibrium where lighter fluid tends to rise to the top of the heavier fluid. **The bubble then bifurcates into smaller structures called Equatorial Plasma Irregularities. The growth rate of the R- T instability is given by the simplified Equation (1)** (Sultan 1996).

$$\gamma_{FT} = \left(\frac{1}{L_{FT}}\right)\left(\frac{\Sigma_P{}^F}{\Sigma_P{}^F+\Sigma_P{}^E}\right) \mathrm{x} \left(\frac{E}{B} - U^P{}_{FT} + \frac{g}{\nu_{in}}\right) - \beta_{FT} \qquad (1)$$

Event 1: 19 December 2022

- Super EPB detected by Swarm A/C ~10:27 -10:30 UT
- Extended below -28° Mlat (Fig 2c)
- (Fig 2b) Sustained increase in Te ~1 minute with a peak of ~2.8x10^3 K
- Fluctuations in Rate of TEC Index (Fig 2a) with a peak of ~0.2 TECU/s
- Solar wind geomagnetic conditions (Fig 3): during a minor storm with a SYM-H (d) minimum around -40 nT during the time of the Super EPB detection
- Bz negative
- Flow speed ~320 km/s
- (Fig 4) shows two TEC maps before (a) and after (b) detection by by SWARM A/C
- The EPB extended up through the equator in a C-shape typical of EPBs (southern hemisphere TEC affected by fitting)
- Super EPB expanded after forming around 08:42 UT

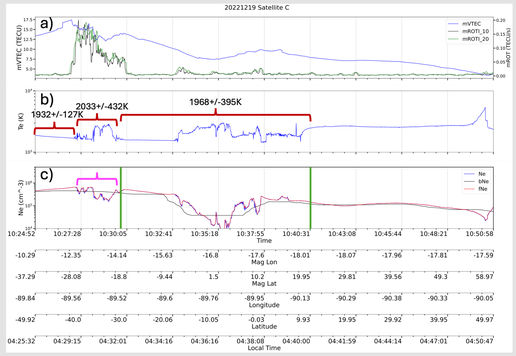

Figure 2. Swarm C satellite data for 19 December 2022 showing vertical TEC and ROTI (a), Te with μ±σ (b), and electron density (c) the pink bracket show the Super EPB and the green vertical lines +/- 20° Mlat

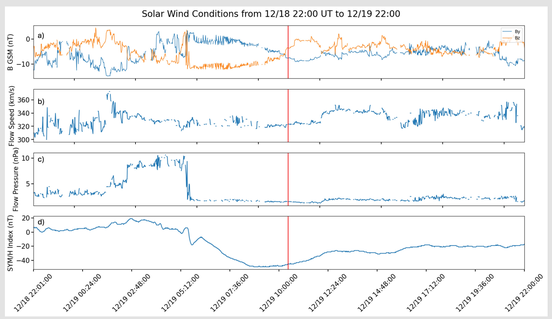

Figure 3. Solar wind data from NASA OMNI showing the B field (a), flow speed (b), Flow pressure (c), and SYM-H index (d). Super EPB swarm detection shown by red vertical line

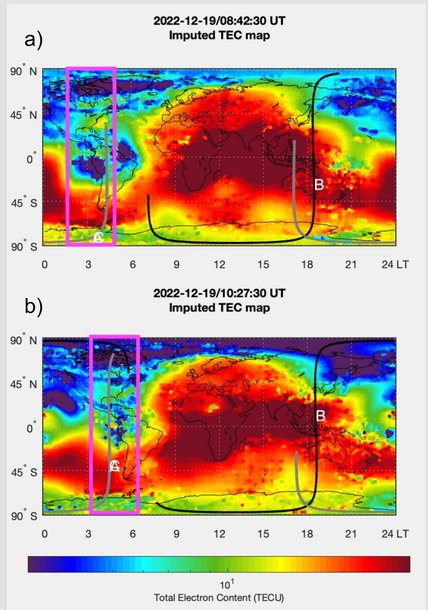

Figure 4. VISTA TEC (Sun et al., 2022, 2023) maps of the Super EPB shown in the pink box first spotted by Swarm A/C ~10:27 UT. Swarm A/C trajectory shown in gray

Event 2: 27 February 2023

- Super EPB detected by Swarm A ~00:25 -00:28 UT
- Extended below -25° Mlat (Fig 5c)
- Minor temperature spikes (Fig 5b) with a peak of ~2.2x10^3 K.
- Fluctuations in Rate of TEC Index (Fig 5a) with a peak of ~0.25 TECU/s
- Solar wind and geomagnetic conditions (Fig 6): beginning of a strong storm with the SYM-H index (d) decreasing ~-150 nT ~12 hours after the Super EPB was detected
- Bz negative
- Flow speed ~700 km/s
- (Fig 7) shows a large Super EPB to the right of the magenta lines just before Swarm A detection
- Extends beyond the EIA crests

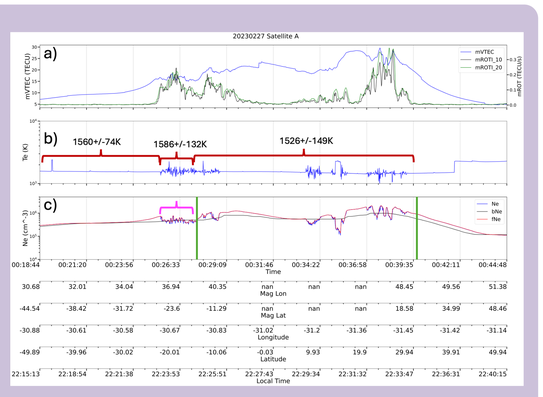

Figure 5. Swarm A satellite data for 27 February 2023 showing vertical TEC and ROTI (a), Te with μ±σ (b), and electron density (c) the pink bracket show the Super EPB and the green vertical lines +/- 20° Mlat

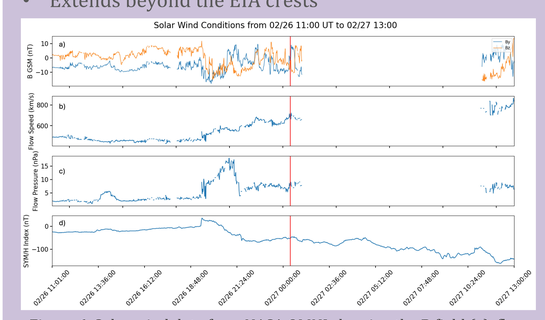

Figure 6. Solar wind data from NASA OMNI showing the B field (a), flow speed (b), Flow pressure (c), and SYM-H index (d). Super EPB swarm detection shown by red vertical line

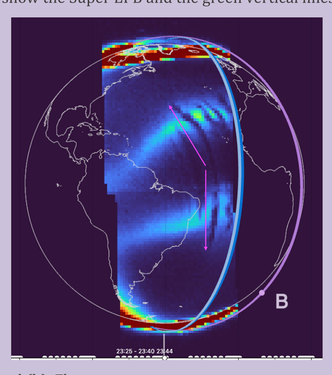

Figure 7. GOLD atomic oxygen emissions for 26 February 2023 23:44 UT (https://spaceweather.knmi.nl/viewer/?layout=swarm_switch_gold#start=2023-03-15T20:21:48&end=2023-04-01T04:29:55)

Event 3: 24 March 2023

- Super EPB detected by Swarm B ~03:46 -03:48 UT and then again between ~04:00-04:01 UT
- Extended above 30° Mlat below -27 ° Mlat (Fig 8c)
- Minor temperature variations (Fig 8b) that fluctuate quickly with one sustained burst ~ 30 seconds
- Temperature peak ~ 3x10^3 K
- Fluctuations in Rate of TEC Index (Fig 8a) with a peak of ~0.3 TECU/s
- Solar wind and geomagnetic conditions (Fig 9): strong geomagnetic storm with a SYM-H (d) minimum of below -150 nT just before the Super EPB detection by Swarm B
- Flow speed ~450 km/s
- Bz negative
- (Fig 10) shows the TEC map of the Super EPB just before it was spotted (a) by Swarm B and just after the second detection (b)
- Exhibits characteristic C-shape

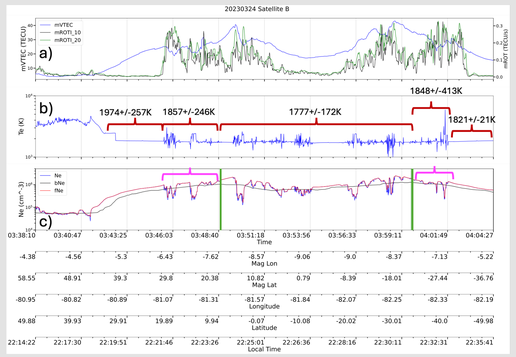

Figure 8. Swarm B satellite data for 24 March 2023 showing vertical TEC and ROTI (a), Te (b), and electron density (c) the pink bracket show the Super EPB and the green vertical lines +/- 20° Mlat

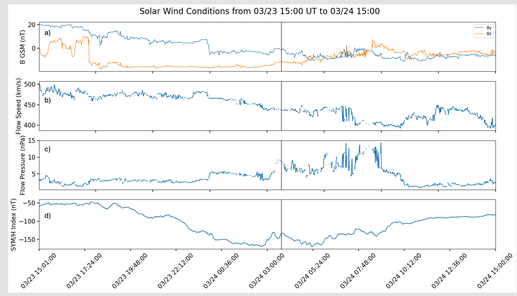

Figure 9. Solar wind data from NASA OMNI showing the B field (a), flow speed (b), Flow pressure (c), and SYM-H index (d). Super EPB swarm detection shown by red vertical line

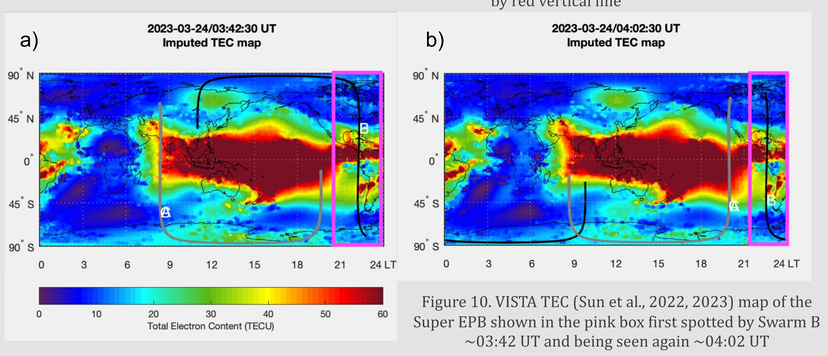

Figure 10. VISTA TEC (Sun et al., 2022, 2023) map of the Super EPB shown in the pink box first spotted by Swarm B ~03:42 UT and being seen again ~04:02 UT

Comparing the Super EPBs

To better understand the nature of Super EPBs, it is important to compare the available data. There are limitations due to data availability and what part of of the EPB Swarm passed through. However, a solid analysis is still able to be completed.

	Similarities	Differences
Solar Wind Conditions	• At time of Swarm detections, Bz was negative	• For Event 2, Bz varied more • Different flow speeds
Geomagnetic Activity Conditions	• All events occurred during geomagnetic storms • There was storm enhanced density (SED)	• Events occurred during storms of different strengths • Strongest storm: Event3 • Weakest storm: Event 1 • Event 2 occurred before the SYM-H minimum
EPB Properties	• Fluctuations in Te and ROTI • Events 2 and 3 are postsunset EPBs	• Stronger TEC for Event 3 • The EPB depletion was deeper for Event 1 and 3 than Event 2 • Event 1 had a larger, more sustained temperature variation

Discussion of Te

One important parameter to explore is the Te detected by SWARM below, within, and above the Super EPB. The mean and standard deviations are shown in Figs 1b,5b, and 8b above red brackets indicating time range. It can be noted that the Te mean and standard deviation for the Super EPB are comparable to low Mlats except for the 2nd spotting of the Super EPB in Event 3. In Event 1, the mean Te and the standard deviation are smaller before the Super EPB. However, this is not true for Events 2 and 3. This could be due to a temperature spike before the EPB potentially as a part of the midlatitude trough. Without these spikes, the results are similar to Event 1. It can be suggested that Super EPBs are comparable in electron temperature to regular EPBs spotted by SWARM in the same trajectory.

Discussion

In Equation (1), the second term in parentheses indicates that the growth rate is larger when the E region disappears in the nighttime hours, which is why EPBs occur most often during postsunset and postmidnight hours. The ion-neutral collision frequency (ν_{in}) decreases with the uplift of the F layer increasing Equation (1), which occurs when the PRE zonal electric field increases the drift after sunset during quiet times (Aa et al., 2020a; Abdu, 2005; Carter et al., 2013; Fejer et al., 1999; Kil, 2015; Woodman & La Hoz, 1976).

Geomagnetic storms have the potential to enhance EPBs because of the prompt penetration electric field (PPEF) that can occur. PPEF is caused when the IMF Bz turns southward causing enhanced solar wind-magnetosphere coupling. This can aid in the rate of occurrence of duskside EPBs by enhancing the zonal electric field (Aa et al., 2019; Abdu et al., 2003; Basu et al., 2001, 2007; Huang et al., 2010; Ram Tulasi et al., 2008). While the postsunset EPBs are correlated positively with solar activity, postmidnight EPBs have a negative correlation (Aa et al., 2020b).

The Super EPBs shown in this analysis occur during geomagnetic storms during southward IMF, which aided in their growth into Super EPBs from the PPEF. The two EPBs that occurred during postsunset hours occurred during strong geomagnetic storms. Although Aa et al. (2020b) found that postmidnight EPBs have a negative correlation with solar activity, Event 1 still grew into a Super EPB possibly because it occurred during a mild geomagnetic storm and not a stronger one.

Although these EPBs have many similarities, it is also important to note the differences. Event 2 occurred during the early main phase of the storm, while Events 1 and 3 occurred solidly during the main phase. Additionally, the flow speeds and flow pressures of the solar winds had different strengths. **Super EPBs may occur under a variety of solar wind plasma conditions.**

Conclusions and Future Work

Super EPBs are a newly studied phenomenon that have far-reaching implications for satellite communications at midlatitudes. It is important to study how often this phenomenon occurs and under what solar and geomagnetic activity conditions that cause such an expansion are and the scintillations they induce. This multi-event analysis is a starting point for understanding Super EPBs. Shown in this analysis are the conditions under which three Super EPBs occurred and their properties. Notably, the Bz was negative, there were different temperature variations, and they occurred during storms.

We plan to study these events further to find the seeding mechanisms and conduct more detailed analyses . In the future we plan to develop an algorithm that detects Super EPBs from Swarm satellite data ranging from 2013 to 2024. With that information, we will conduct a statistical analysis on Super EPBs.

Acknowledgements and References

AC was supported by NASA FINESST 80NSSC22K1847

Aa et al., (2020a). Coordinated ground-based and space-based observations of equatorial plasma bubbles. *Journal of Geophysical Research: Space Physics.*

Aa et al., (2020b). Statistical analysis of equatorial plasma irregularities retrieved from Swarm 2013–2019 observations. *Journal of Geophysical Research: Space Physics.*

Abdu, M.A. (2019) Day-to-day and short-term variabilities in the equatorial plasma bubble/spread F irregularity seeding and development. *Prog Earth Planet Sci.*

Basu et al., (2001). Response of the equatorial ionosphere in the South Atlantic Region to the Great Magnetic Storm of July 15, 2000. *Geophysical Research Letters.*

Basu et al., (2007). Response of the equatorial ionosphere at dusk to penetration electric fields during intense magnetic storms. *Journal of Geophysical Research.*

Carter et al., (2013). On the occurrence of equatorial F-region irregularities during solar minimum using radio occultation measurements. *Journal of Geophysical Research: Space Physics.*

Fejer et al., (1999). Effects of the vertical plasma drift velocity on the generation and evolution of equatorial spread F. Journal of Geophysical Research.

Huang et al., (2010). Storm time electric fields in the equatorial ionosphere observed near the dusk meridian. *Journal of Geophysical Research.*

Kil, H. (2015). The morphology of equatorial plasma bubbles—A review. *Journal of Astronomy and Space Sciences.*

Ram Tulasi et al., (2008). Local time dependent response of postsunset ESF during geomagnetic storms. *Journal of Geophysical Research.*

Sultan, P. J. (1996). Linear theory and modeling of the Rayleigh-Taylor instability leading to the occurrence of equatorial spread F. *Journal of Geophysical Research.*

Sun et al., (2023). Complete global total electron content map dataset based on a video imputation algorithm VISTA. *Scientific Data.*

Sun et al., (2022). Matrix completion methods for the total electron content video reconstruction. *Annals of Applied Statistics.*

Woodman, R. F., & La Hoz, C. (1976). Radar observations of F region equatorial irregularities. *Journal of Geophysical Research.*

Yokoyama et al., (2014). Nonlinear growth, bifurcation, and pinching of equatorial plasma bubble simulated by three-dimensional high-resolution bubble model. Journal of Geophysical Research.